P. Gajan, F. Simon, M. Orain, V. Bodoc
(ONERA)

E-mail: Pierre.Gajan@onera.fr

DOI : 10.12762/2016.AL11-09

Investigation and Modeling of Combustion instabilities in Aero Engines

Combustion instability results from a coupling between acoustic and heat release fluctuations. From the analysis of published works by various research teams including ONERA, this paper describes the coupling lines involved, the model used to describe it and the methods developed to predict the thermo-acoustic risks. The application is focused on the liquid-fueled aero engine specificities. Recent results obtained at ONERA on the influence of the liquid flow behavior on these couplings are described and compared with LES results.

Introduction

Confined devices with an internal heat source are predisposed to thermo-acoustic instabilities, resulting from a coupling between the acoustic field, pressure and velocity fluctuations (respectively p' and u'), and the unsteady heat release (q'). This phenomenon was first observed by Higgins [1] and Rijke [2] and explained by Lord Rayleigh in 1878 [3]. During the second half of the 20th century, many studies were first focused on instabilities occurring in liquid propellant rockets [4] and later in other combustion devices such as industrial furnace, boilers or other propulsion systems like solid rockets, gas turbines or afterburners. For these different applications, the coupling line between the acoustic components and the unsteady heat release greatly depends on the combustion regime (premixed or not), the reactant characteristics and state (solid, liquid or gaseous) and the injection procedure. In the same way, the feedback loop between the unsteady heat release and the acoustic state depends on the device geometry, its boundary conditions and the Mach number distribution. As a result, each configuration induces specificities that must be taken into account.

Over the last few decades, many studies on combustion instabilities have concerned land-based turbine or aero engines. In these fields (energy production or civil air transport), manufacturers try to reduce the environmental impact by modifying their engine concept. In particular, over the past two decades, they have been developing shorter combustion chambers operating at higher OPR (Overall Pressure Ratio) in lean combustion regimes, in order to minimize pollutant formation (NOx, soot, etc.). In these new combustors, a higher air mass flow rate is required for the combustion; therefore, less air is available for cooling the combustor walls. Consequently, walls with multiple perforations are generally used for cooling, which modifies their acoustic impedance. Some of these geometric modifications may enhance the onset of combustion instabilities, which lead to large cyclic pressure or velocity fluctuations inside the chamber and consequently generate significant heat transfer at the combustor walls, or large amplitude vibrations of the structure. This can result in the damaging of the combustor, or even its destruction, which is incompatible with the safety and durability standards required in the aeronautical industry.

The aim of this paper is to present the recent developments, in particular at ONERA, on combustion instabilities encountered in aero engines. In the first section of this paper, the main mechanisms involved in the $p'\,q'$ coupling are described, with a specific focus on liquid-fueled devices. The different approaches used to model this coupling and to predict the instability onset are presented in the second and third sections respectively. Their application on the ONERA setup LOTAR (Liquid Fueled ONERA ThermoAcoustic Rig) is then discussed.

Description of the main mechanisms involved in the $p'q'$ coupling

The coupling can be described as a closed loop of interactions, back and forth, between acoustic components and heat release, as schematically represented in Figure 1. It was shown in the works of Putman and Dennis [5], or Nicoud and Poinsot [6] that the flame stability depends on an extended Rayleigh criterion, which compares the source term of acoustic energy from the flame with the acoustic fluxes at the boundary surfaces, as shown in Eq. (1). The source term depends on the phase relationship between pressure and heat release oscillations in the combustor, which is imposed by the different time delays appearing in the p'-q' coupling.

$$\frac{1}{T}\int_T \left\{ \frac{\gamma-1}{\gamma\,\overline{p}} \iiint_\Omega p'\,q'\,dV - \oiint_\Sigma p'\,u'\,dA \right\} dt > 0 \qquad (1)$$

In Eq. (1), γ is the heat capacity ratio; p', u', q' are respectively the pressure, velocity, and heat release rate fluctuations; T is the instability cycle period; $\overline{p}$ is the average pressure over the system control volume, Ω; Σ is the system control surface; and, finally, dV and dA are respectively the volume and surface integration variables.

This equation states that the acoustic energy increases only if the source term due to combustion is larger than the acoustic losses on the combustor inlet and outlet surface Σ. The experimental evaluation of acoustic fluxes on the boundaries of the burner is difficult and less attention has been paid in the literature to their influence. Nevertheless, experimental methods based on multiple-microphone measurements or *LDA* and microphone measurements are used to identify such losses in the case of liners enabling acoustic energy to be damped inside of aero engines [7].

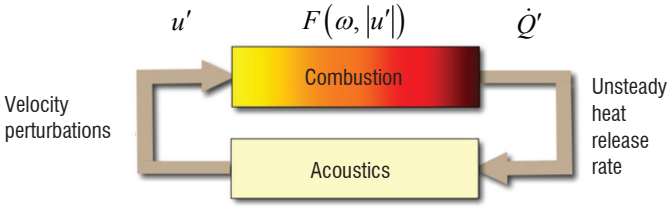

Figure 1 - Coupling loop at the origin of thermo-acoustic instabilities

Pressure fluctuation production from the flame

On the lower side of the coupling loop presented in Figure 1, unsteady heat release produces pressure (or velocity) fluctuations. The fundamental mechanism involved in the sound generation is the unsteady gas expansion induced by heat release fluctuations [8-10]. Similarly, it was shown by Marble and Candel [10], Polifke et al. [12], and Huet and Giauque [12] that pressure fluctuations could arise when entropy or vorticity waves, coming from the unsteady flame or upstream flow, interact with an abrupt modification of the flow cross-section. Note that, in most cases, the Mach number in the combustor being low, the convection of entropy or vorticity waves induces large time delays between the unsteady heat release, q', and the pressure fluctuations, p', in comparison with the time scale associated with the direct acoustic perturbation produced by the flame. It must be noticed that the relevance of such waves in the pressure production depends greatly on their dispersion rate between the reactive zone and the combustion chamber outlet. In particular, Sattelmeyer [14] showed that the related convection time limits this effect in many applications.

The acoustic pressure and velocity fluctuations propagate in the volume domain and interact with the boundary surface leading either to energy losses or reflection, depending on their own frequency and propagation mode and the local conditions (Mach number, surface characteristics, etc.). According to the flow characteristics (temperature, Mach number) and the boundary conditions, standing or spinning waves characterized by their wavelength, spatial distribution and amplitude take place in the volume domain. They correspond to particular eigenmodes, which can be deduced from an acoustic analysis based on the Helmholtz equation or linearized Euler equations [15-17].

Origins of heat release fluctuations

On the upper side of the loop, the production of heat release fluctuations from p' or u' is not so clear and depends upon the characteristics of the combustion system. In premixed flames, local modifications of the flame area induced by turbulent or vortical structures, or wall interaction, control the mixing between fresh and unburned gases and consequently the reaction rate in the flame [9]. In their configuration, Noiray et al. [17] observed that these flame surface variations are induced by upstream velocity oscillations. Gutmark [18] reviewed the main mechanisms linking the heat release fluctuations to vortical structures formed in shear layers. These structures capture fresh gases or fuel in their center, while the flame is located at their periphery. During interactions between two adjacent structures or with a wall, rapid mixing occurs, which leads to a spot of heat release. Many studies show that the eddy formation in shear layers may be driven by external acoustic excitations. Thus, when the acoustic level increases, a high coupling appears between the acoustic components and the unsteady heat release.

Another source of unsteady heat release originates from the interaction between inhomogeneous equivalence ratio regions and the flame [19]. For a premixed flame, pressure oscillations close to the injection interact with the fuel line and induce an oscillation in the fuel flow rate creating a local modification of the equivalence ratio, which propagates towards the combustion zone [20]. The same phenomena can be also observed with a constant fuel injection rate but oscillating air velocity. This convective transport induces a time delay linked to the fresh gas velocity and the distance between the injection and the flame locations.

Specificity of the liquid fuel flames

In the literature, many articles deal with gas-fueled combustors in premixed or diffusion regimes, in order to describe and model the phenomena considered and to determine the p' (or u') - q' relationship [8, 9]. When a liquid fuel is used, the coupling between the acoustic fluctuations and the unsteady heat release involves additional phenomena, such as spray atomization / transport / vaporization / combustion [21-24] and their interaction with turbulence, vorticity, chemistry, and acoustics. Eckstein et al. [21] analyzed the spray generated by an air-blast system subject to periodic air velocity fluctuations. The authors observed that the droplet size in the spray varied periodically at the same frequency as the velocity excitation. Moreover, they explained that, for a given liquid flow rate, high air velocities produce a large number of small droplets, whereas low air velocities produce a small amount of large droplets. In this way, when combustion instabilities occur, the periodic velocity fluctuations inside the atomizer create a time-varying droplet size distribution, which is transported further downstream to the flame as a droplet wave. During this convection phase, the small-droplet zones produce a larger amount of fuel vapor than the large-droplet zones. As a result, an equivalence ratio wave appears, which interacts with the flame to produce a periodic heat release oscillation.

In parallel, Giuliani et al. [22] and Gajan et al. [23] studied non-reactive spray behaviors downstream both from a simplified atomizer and from a Dextre-type industrial atomizer under non-reactive conditions. In the first case, droplets were formed from the disintegration of an axisymmetric liquid sheet sheared internally and externally by two co-swirling airflows. In the second case, a prefilming zone was formed before the atomization of the liquid fuel. In these experiments, velocity pulsations were created by a siren placed upstream or downstream from the atomizer. In both cases, droplet density waves convected downstream from the fuel injection location are observed (Figure II.2).

Giuliani [25] observed a great interaction between the droplet concentration fronts and the convection of annular vortices formed in the swirling air jet shear layer (Figure 2). A succession of vortex rings followed by a dense droplet front evolving on the surface of the spray envelope is created. The following ring vortex contains only sparse droplets. The measured convection velocity of the droplet density wave is approximately equal to half of the air velocity at the injector outlet.

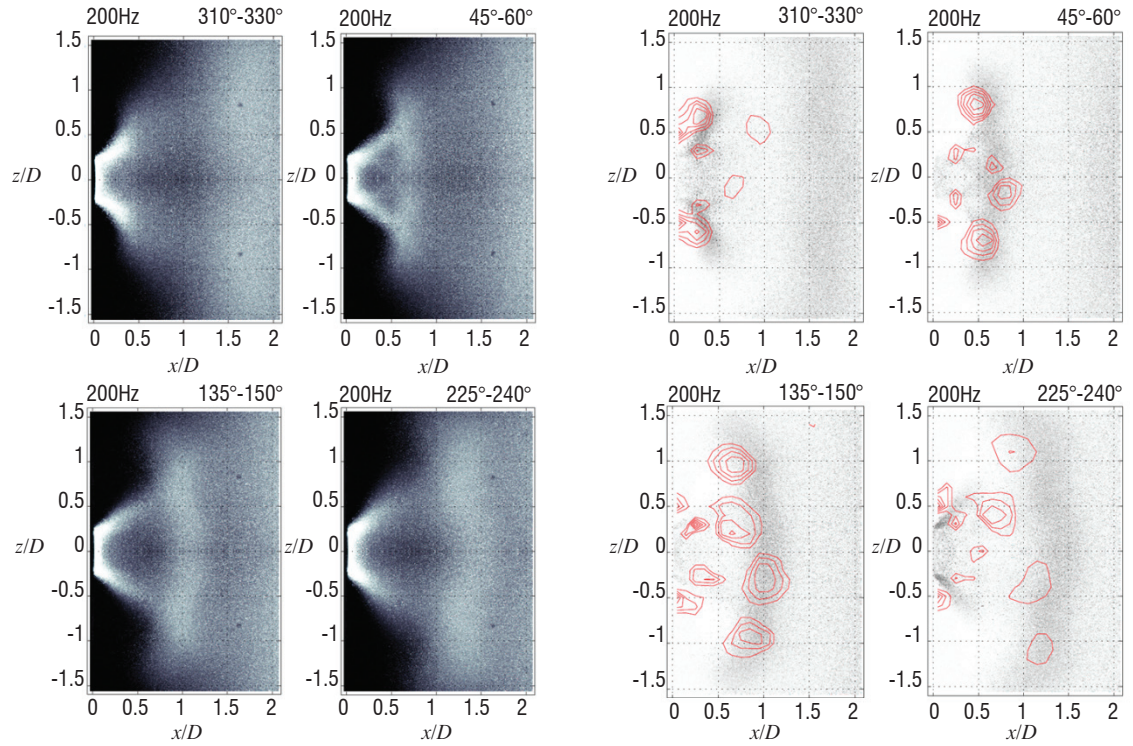

Figure 2 - Phase averaged images obtained of a spray subjected to upstream air pulsation:
Left: Maximum post-processing images, Right : Interaction between the spray and the vortex shedding [22,25](Video 1)

A phase-averaged post-processing method applied to Fraunhofer–Mie scattering or phase Doppler techniques allowed a deep analysis of the origin of these droplet density waves. A typical three-dimensional plotting of the results obtained at one measurement location is shown in Figure 3. The color scales correspond to the axial velocity of the droplets. This figure shows that the excitation imposes a significant modulation of the number of droplets during the cycle, mainly for small droplet sizes. Furthermore, the color scale reveals that the maximum velocity zone is reached between the minimum and the maximum of the droplet population. From these results, the propagation behavior of different droplet size classes was analyzed [23]. It reveals that the convection velocity of these waves depends on the droplet size (Figure 4) and that the wave amplitude increases during the convection phenomena. This last observation concerns mainly the small droplets.

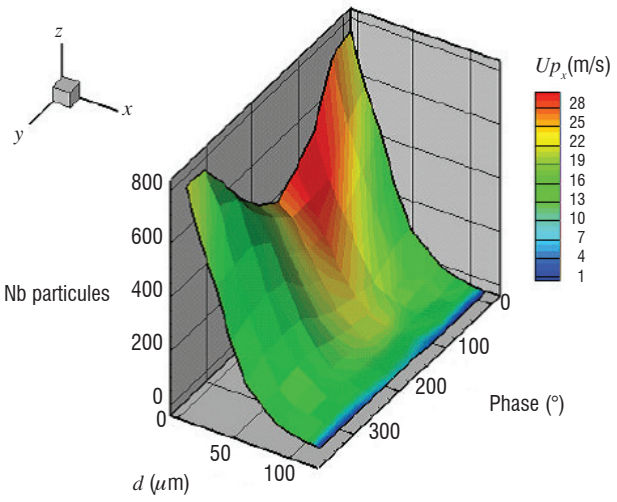

Figure 3 - Evolution of the droplet size histogram along the pulsation cycle [23]; Color levels correspond to the droplet velocity in the longitudinal direction; f =700 Hz, $x/d_{atomizer}$=0:45, $y/d_{atomizer}$=0:45, and $z/d_{atomizer}$=0.

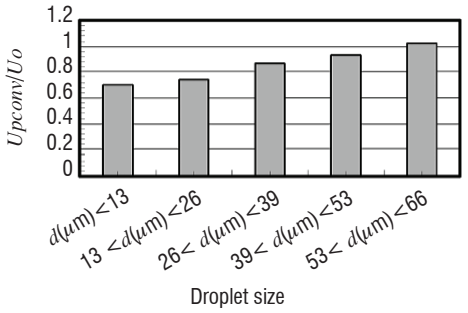

Figure 4 - Averaged convection velocity of the droplet density waves with respect to their size [23].

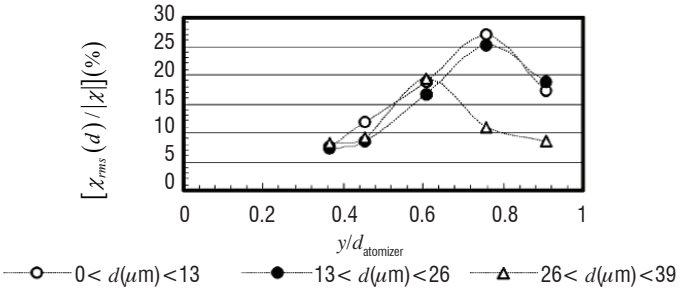

Figure 5 - Amplitude of the number-of-droplet wave at different locations with respect to the droplet size [23].

By using a one-dimensional model based on the Boussinesq-Basset-Oseen (BBO) transport equation, Giuliani et al. [22] and Gajan et al. [23] concluded that this phenomenon was due to the influence of the oscillating velocity field on the motion of the small droplets, which segregates them in space and therefore forms droplet concentration waves (Figure 6). Furthermore, Giuliani et al. [22] noted that the droplets involved had a Stokes number (calculated from the air pulsation period) smaller

than 0.2.The results obtained by this 1D analysis were compared to experimental results by Gajan et al. [23] The amplification phenomena observed experimentally was qualitatively obtained by the simulation (Figure 7).

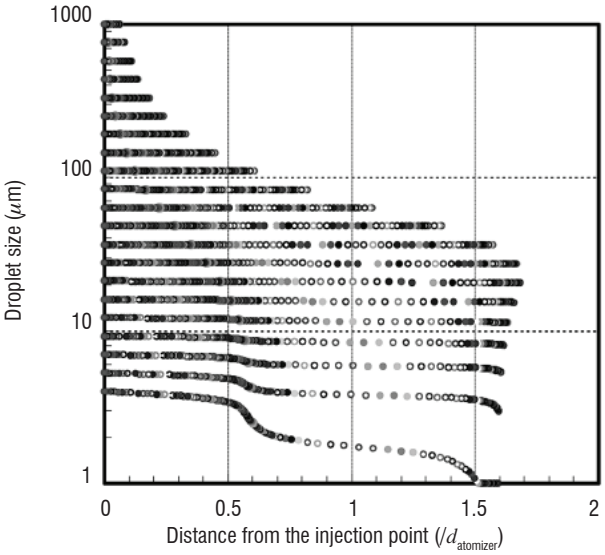

Figure 6 - Instantaneous droplet position and size obtained from the numerical simulation [23].

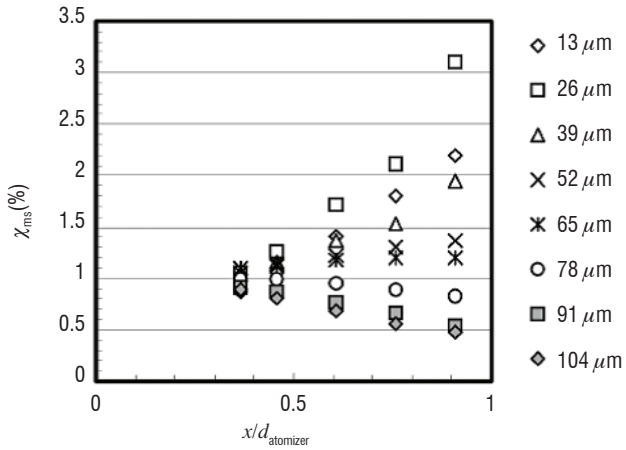

Figure 7 - Amplitude of the droplet concentration wave at different locations with respect to the droplet size [23].

More recently, Apeloig et al. [24] studied the unsteady interaction with the flame of a kerosene spray downstream from a multi-point injector (Figure 8).The injection system comprises two injection zones, a pilot zone composed of a pressure atomizer at the center and a multipoint zone at the periphery. In this zone, the liquid fuel is injected through a set of individual jets in crossflow. Axial and radial swirlers enable air flow rotation to be induced. The distribution of the fuel between the pilot and the multipoint zone is controlled though a Fuel Split Parameter (FSP) corresponding to the percentage of the overall kerosene mass flow rate through the pilot zone.

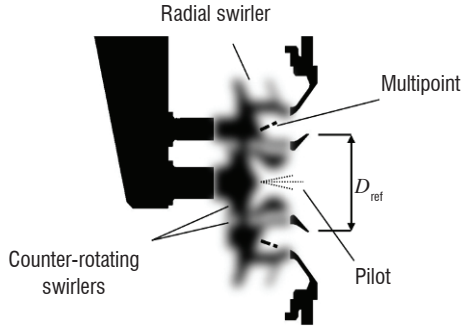

Figure 8 - Schematic diagram of a novel aero-engine injection system used in the experiments [24].

Phase-averaged processing of images obtained from planar laser-induced fluorescence (PLIF) on kerosene reveals that the spray pattern issuing from the multipoint zone fluctuates to a large extent, both spatially and in terms of fluorescence intensity, over the instability cycle (Figure 9). From the analysis of this sequence of images Apeloig et al. [24] defined three main characteristics of the spray dynamics and proposed that the spray behavior is linked to airflow fluctuations inside the injector, which modify the individual trajectories of the fuel jets. Such coupling between the air flow and the jet in the crossflow atomization process was shown by Anderson et al. [26] [Figure 10] and by Song and Lee [27]. When the momentum flux of the crossflow is greater than the momentum flux of the liquid jet ($J<1$), the atomization process results in the liquid jet and droplets hitting the inner wall of the radial swirler, producing a liquid film that is subsequently atomized at the edge of the diffuser. This phenomenon corresponds to a characteristic time, τ_1. When the momentum ratio J reaches a large enough value, the kerosene jet hits the outer wall of the radial swirler, forming a liquid film which is re-atomized further downstream,

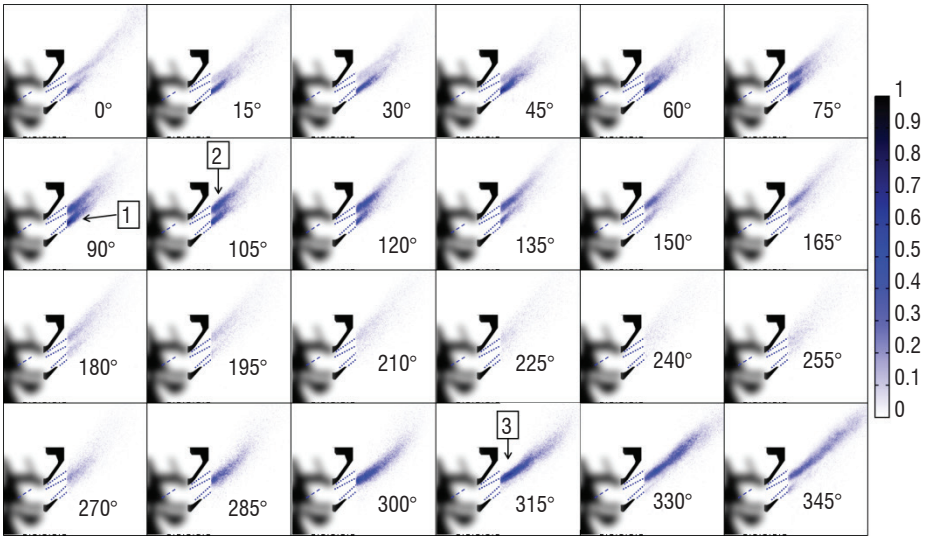

Figure 9 - Temporal sequence of the liquid kerosene spatial distribution during an instability cycle using phase-averaged analysis on PLIF images [24] (Video 2)

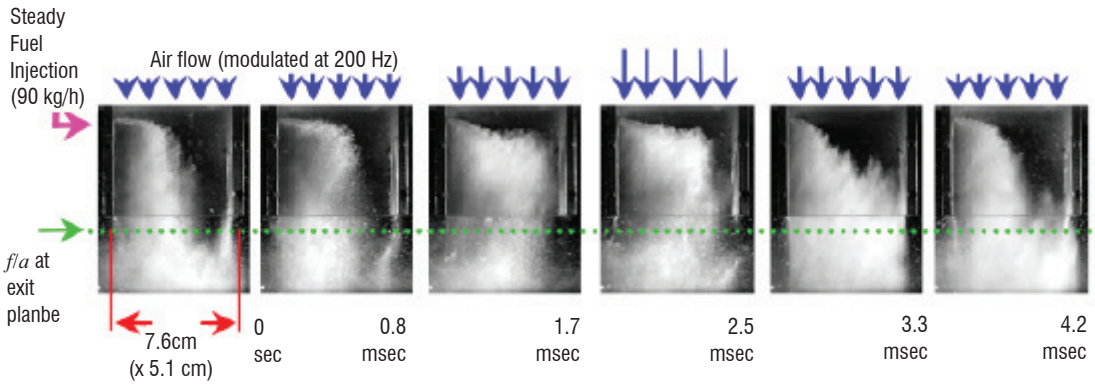

Figure 10 - Instantaneous frame sequence showing the effect of airflow modulation on a steady fuel jet in crossflow [26].

as well as generating droplet rebounds at the wall. This second step corresponds to a characteristic time, τ_2. The third spray pattern, with a characteristic time τ_3, requires further investigation: it may be that liquid fuel is directly transported to the combustor without hitting the walls of the multipoint circuit, and/or a combination of the two previous flux patterns. Different characteristic times thus appear due to the diverse convective mechanisms involved in the liquid atomization and transport from its injection point inside of the injector (wall filming or droplet transport) to the combustor.

The unsteady behavior of the spray influences the vapor concentration field further downstream, creating equivalence ratio fluctuations interacting with the flame. Such phenomena were visualized by Apeloig et al. [24] (Figure 11) indicating highest concentration levels around the liquid phase. In this figure, large fluctuations of the spatial distribution of kerosene vapor are also observed in terms of surface covered and trajectory. Spatial averaging of each phase-averaged field shows the temporal relationship between the different phenomena (Figure 12). In particular, it is evident that the OH emission fluctuations from the flame representative of heat release behavior are directly linked to the unsteady atomization process.

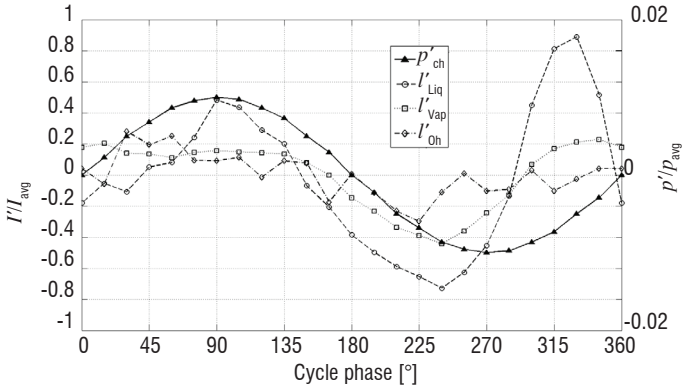

Figure 12 - Temporal sequence of the OH radical and kerosene fluorescence intensities during an instability cycle using phase-averaged analysis on PLIF images [24].

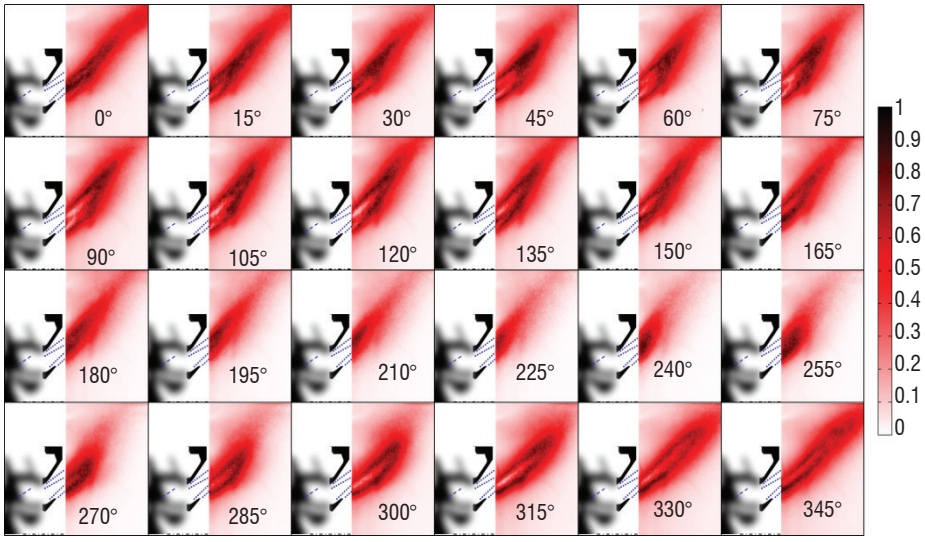

Figure 11 - Temporal sequence of the kerosene vapor spatial distribution during an instability cycle using phase-averaged analysis on PLIF images [24](Video 3).

Methods for defining the flame response to acoustic perturbations

The key point to predict combustion instabilities is the modeling of the flame response to acoustic perturbations. As shown in the previous section, various phenomena are involved in this response. Nevertheless, from a macroscopic point of view, this response was described through two parameters corresponding to the interaction degree and the time delay between the acoustic incident perturbation and the behavior of the flame. These two parameters were introduced by Crocco and Cheng [28] in their well-known n-τ model. In the frequency domain, these parameters correspond to the amplitude and the phase of the Flame Transfer Function (FTF), which depends on the frequency. These two approaches suppose that the flame response is linear, i.e., that it is proportional the excitation level. Although they can accurately describe the different instability modes, they cannot predict the limit cycle phenomena corresponding to a saturation effect when the amplitude of the excitation increases. In order to improve the prediction tool efficiency, many authors have proposed nonlinear models to describe the flame behavior [14, 15]. Illingworth and Juniper [29] analyzed this approach to represent the nonlinear behavior of the flame

Flame transfer function

The simplest flame transfer function corresponds to the n-τ model proposed by Crocco and Cheng [28]. It can be written in the frequency and temporal domain as follows [30]:

$$\frac{\gamma-1}{\rho_{up}c_{up}^2}\hat{Q}=S_{up}\cdot n\cdot\hat{u}\left(x_f\right)e^{-i\omega\tau_f}$$

$$\Leftrightarrow\frac{\gamma-1}{\rho_{up}c_{up}^2}Q(t)=S_{up}\cdot n\cdot u\left(x_f,t-\tau_f\right)$$

Where $Q(t)=\int_{x_{up}}^{x_d}S\cdot q'dx$ is the total unsteady heat release produced by the flame, n is the interaction index and τ_f is the flame time delay. The subscript "up" corresponds to conditions upstream from the flame and ($\hat{}$) to the Fourier transform. Bloxsidge et al. [31] added a second time scale, in order to take into account the damping phenomena that appear at high frequencies. A first order response can be written.

$$\frac{\gamma-1}{\rho_{up}c_{up}^2}\hat{Q}=\frac{S_{up}\cdot n\cdot\hat{u}\left(x_f\right)}{1+i\omega\tau_1}e^{-i\omega\tau}$$

$$\Leftrightarrow\frac{\gamma-1}{\rho_{up}c_{up}^2}\left(\tau_1\frac{d}{dt}+1\right)Q(t)=S_{up}\cdot n\cdot u\left(x_f,t-\tau\right)$$

Dowling [15] used a third time scale, in order to reproduce the behavior of the flame with a second order response law.

$$\frac{\gamma-1}{\rho_{up}c_{up}^2}\hat{Q}=\frac{S_{up}\cdot n\cdot\hat{u}\left(x_f\right)}{\left(1+i\omega\tau_1\right)\left(1+i\omega\tau_2\right)}e^{-i\omega\tau}$$

$$\Leftrightarrow\frac{\gamma-1}{\rho_{up}c_{up}^2}\left(\tau_1\frac{d}{dt}+1\right)\left(\tau_2\frac{d}{dt}+1\right)Q(t)=S_{up}\cdot n\cdot u\left(x_f,t-\tau\right)$$

The above approaches were mainly applied for premixed flames or assumed that equivalence ratio fluctuations can be neglected. As shown in the previous section, equivalence ratio fluctuations can be the main mechanism at the origin of the p' q' coupling. Lieuwen and Zinn [20] introduced the effect of these fluctuations in their flame response. They supposed that the equivalence ratio fluctuation produced near the fuel injection location is convected without diffusion toward the flame location. Therefore, in their model, a convective time τ_c proportional to the distance between these two locations and inversely proportional to the gas bulk velocity is used. Sattelmayer [14] takes into account the fuel diffusion through the following expression :

$$\frac{\varphi'_f}{\varphi'_{inj}}=\frac{1}{2\cdot\Delta\tau_c\cdot i\cdot\omega}\cdot e^{-i\omega\bar{\tau}_c}\left(e^{i\omega\Delta\tau_c}-e^{-i\omega\Delta\tau_c}\right)$$

In their application, the fuel line is choked, therefore the equivalence ratio fluctuation produced near the injection point is directly proportional to the local acoustic velocity. The response of the flame to these equivalence ratio fluctuations is given by Lieuwen [10] and is decomposed through two terms linked to the reaction heat and the flame speed perturbations respectively:

$$\frac{Q'}{\bar{Q}}=n_H\varphi'_f+n_S\frac{d\varphi'_{inj}}{dt}\quad\text{with}\quad n_H=\left.\frac{d\left(\Delta h'_R/\Delta\bar{h}_R\right)}{d\varphi}\right|_{\bar{\varphi}}$$

$$\text{and}\quad n_S=\frac{1}{3}\frac{L_F}{\bar{u}}\left.\frac{d\left(S'/\bar{S}\right)}{d\varphi}\right|_{\bar{\varphi}}$$

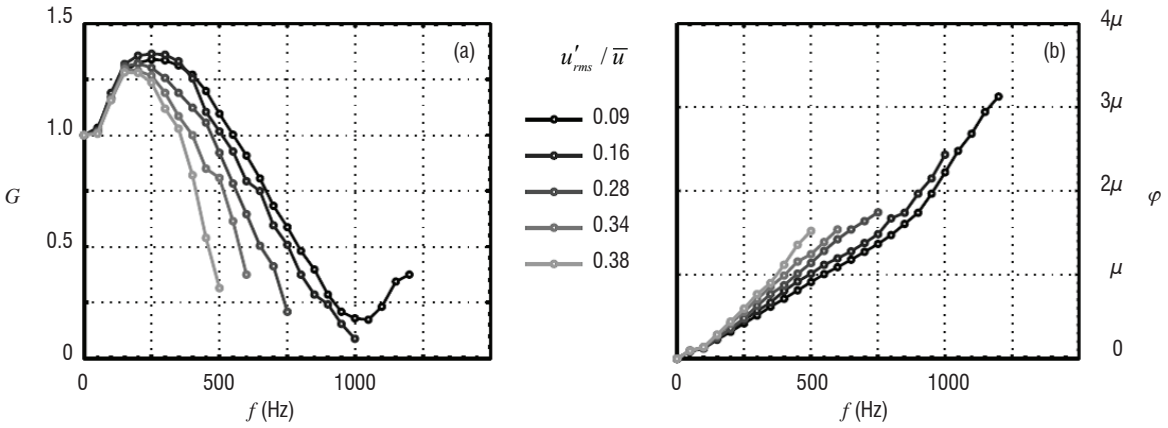

Figure 13 - Experimental flame transfer function for different normalized driving velocity amplitude rates. (a) Gain G. (b) Phase φ [17]

Flame describing function

In order to analyze, for a given system, the risks linked to thermoacoustic oscillations, it is important not only to define the linear frequencies and growth rates, but also to predict the amplitude and frequencies at the limit cycles. Various works were carried out first to explain and then to model the phenomena at the origin of these nonlinear behaviors. They used the describing function approach used in other application fields. The method treats the nonlinear element in a quasi-linear approach when sinusoidally forcing an induced nonlinear response. The response of the system depends both on the input frequency and amplitude. Dowling [16] represents the premixed flame response behind flame holder experiments by Langhorne et al. [32] through three upstream velocity conditions. For a negative upstream velocity, the flame vanishes ($q'=0$), the u' q' relationship is linear for velocities between 0 and two times the upstream bulk velocity, and finally q' saturates for higher velocities. Illingworth and Juniper [29], using the same approach, show that this nonlinear flame description generates harmonics.

A detailed analysis of the linear and nonlinear behavior of a burner formed by 420 elementary flames operating in the premixed regime is presented by Noray et al. [17]. The flame describing function obtained with this setup exhibits a clear dependence of the flame response on both the frequency and the amplitude of the velocity excitation.

Methods for predicting instability combustion risks

Low order methods

Various teams developed this method to predict the acoustic response of a given system. They are based on the linear acoustic approach. A multiport approach, which represents the system as a network of individual elements connected each other by jump conditions. A linear system of equations is constructed from the transfer matrices between two successive elements or between the inlet and the outlet of each element [30, 33]. The following relationship is obtained:

$$\begin{pmatrix} p'_{i+1} \\ u'_{i+1} \\ \phi'_{i+1} \\ ?. \end{pmatrix} = \begin{bmatrix} T_{pp}(\omega) & T_{pu}(\omega) & T_{p\phi}(\omega) & T_{p?}(\omega) \\ T_{up}(\omega) & T_{uu}(\omega) & T_{u\phi}(\omega) & T_{u?}(\omega) \\ T_{\phi p}(\omega) & T_{\phi u}(\omega) & T_{\phi\phi}(\omega) & T_{\phi?}(\omega) \\ T_{?p}(\omega) & T_{?u}(\omega) & T_{?\phi}(\omega) & T_{??}(\omega) \end{bmatrix} \begin{pmatrix} p'_i \\ u'_i \\ \phi'_i \\ ?. \end{pmatrix}$$

The flame response is introduced through the acoustic pressure and velocity jump across the flame zone. For this, the flame transfer function described before can be used. For compact flames, the acoustic jump across the combustion zone can be deduced from the integration of the linearized mass, momentum and energy balance equations [30]. This imposes that the acoustic pressure is continuous across the flame and the acoustic velocity jump is equal to:

$$S_{down}\hat{u}_{down} - S_{up}\hat{u}_{up} = \frac{\gamma - 1}{\rho_{up}c_{up}^2}\hat{Q}$$

Coupling all of the individual matrices, the overall system of linear equations is obtained [33]:

$$\overline{\overline{G}}(\omega).\vec{M} = \vec{0}$$

The dimension of the square matrix $\overline{\overline{G}}$ depends on the number of individual elements taken into account to represent the whole system and on the number of unknown variables of the problem. $\vec{M}$ is a vector containing all of the unknown variables. The complex eigenmodes of the system are obtained by solving the following equation:

$$\det(\overline{\overline{G}}(\omega)) = 0$$

The stability of the various eigenmodes $\omega = \omega_R + i \cdot \omega_I$ is obtained through the growth rate parameter GR [33]:

$$GR = e^{-2\pi\frac{\omega_I}{\omega_R}}$$

Where GR=1 represents the stability limit of a linear system or the limit cycle of a nonlinear system. In linear systems, GR<1 indicates stable modes, while GR>1 corresponds to unstable modes. From the use of the flame describing function concept, Noiray et al. [17] described the behavior of their setup for different overall lengths and velocity amplitudes. For some modes, a positive growth rate ω_i is obtained for small velocity amplitude levels, but vanishes for higher amplitudes, leading to a stable flame. For other modes, negative growth rates, obtained for small amplitudes corresponding to a linear stable mode, become positive above a certain amplitude threshold, reaching a maximum before decreasing and then vanishing for higher excitation values. The first behavior type induces a saturation effect corresponding to a limit cycle observed in many studies. Noiray et al. [17] have shown that the combination of these two behavior types is at the origin of the frequency jump observed experimentally for fixed setup lengths or the hysteresis phenomena obtained by increasing or decreasing this length.

CFD approach

Helmholtz solvers are used to calculate the eigenmode of linear vibrating systems. This approach is applied in acoustics for complex geometries, or to accurately take into account the temperature field and boundary conditions. For combustion instability purposes, the use of a source term from the flame enables the stable or unstable modes to be defined in the same way as was described for low order methods. These modes are the solution of the following equation [30]

$$\nabla \cdot \left(c_0^2 \nabla \hat{p}\right) + \omega^2 \hat{p} = i\omega(\gamma - 1)\hat{q}(x)$$

As shown before, the unsteady heat release is linked to the velocity fluctuation through the flame transfer or describing function.

Applications to the LOTAR experiment

A schematic diagram of this set-up is presented in Figure 14, where air flows from left to right. It is divided into three parts. The first part (on the left hand side) comprises a siren enabling the rig acoustics to be forced at different frequencies during the Flame Transfer Function (FTF) measurements. A 1 m-long straight pipe, equipped with four microphone taps and two intakes to mount a loudspeaker, is placed between the siren and the plenum of the combustor. The water-cooled combustion chamber is equipped with large windows allowing optical diagnostic applications right at the outlet of the injection system. The last part is a trombone-like section, composed of a fixed tube and a coaxial movable tube. This allows continuous modification of the Inner Exhaust Length (IEL), defined by the length between the exit plane of the injection system and the exit plane of the movable tube. This length change creates a variation of the natural resonant frequencies of the rig. Similarly to the first part upstream from the combustor, this last part is equipped with microphone taps and loudspeaker intakes.

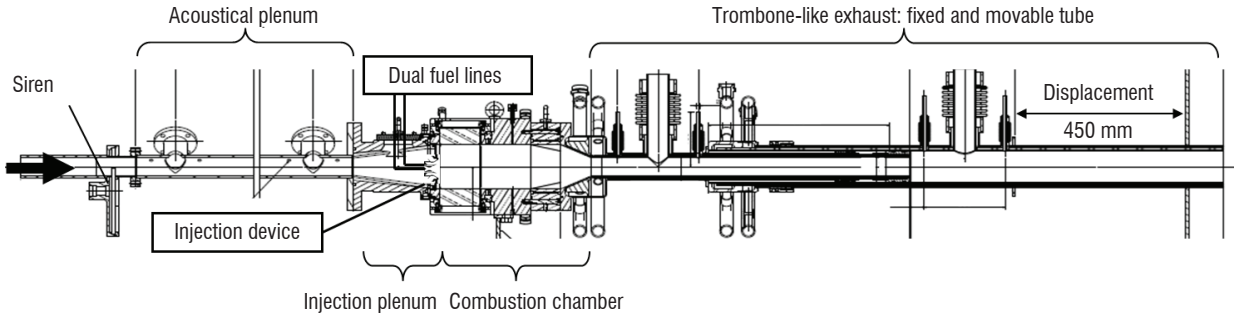

Figure 14 - Schematic diagram of the LOTAR experimental setup (Video 4).

The multipoint injection system used during the test was presented in § "Description of the main mechanisms involved in the p'q' coupling" (Figure 8). Various diagnostic methods, including phase Doppler anemometry, high-speed camera, PLIF and acoustic multiport techniques, were used to investigate the system behavior.

Flame response

Ghani et al. [34] have presented results of the ONERA LOTAR setup obtained from LES simulations with the AVBP code. In this case, the flame transfer function was performed by forcing the inlet velocity at fixed frequencies, with a modulation rate of 15%. The inlet and outlet boundary conditions are imposed through the non-reflecting Navier-Stokes Characteristic Boundary Condition (NSCBC) formulation, which enables acoustic reflection to be controlled. A local transfer function is deduced from the comparison between the local heat release fluctuations and the velocity signal obtained at a reference point located inside the injection system, yet upstream from the radial vane of the swirler (Figure 15). It is shown that the amplitude and time delays depend greatly on the downstream location. By averaging the heat release fluctuation over the volume domain, a global flame transfer function can be determined (Figure 16).

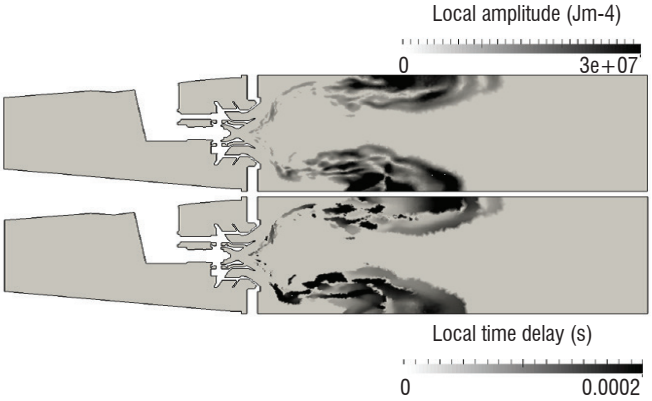

Figure 15 - Local fields of amplitude (top) and time delay (bottom) obtained from CFD (f=220 Hz) [34]

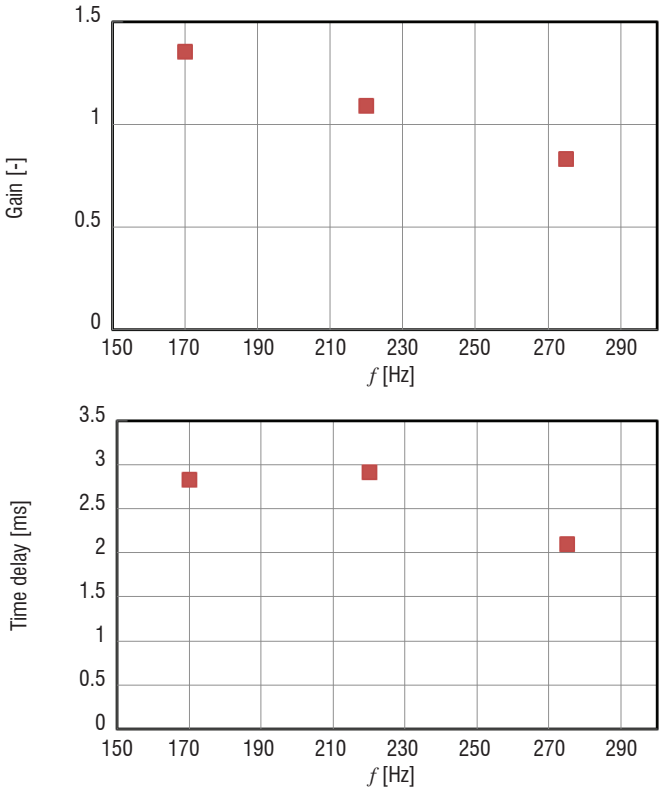

Figure 16 - Gain and Time delay obtained on the LOTAR setup [34].

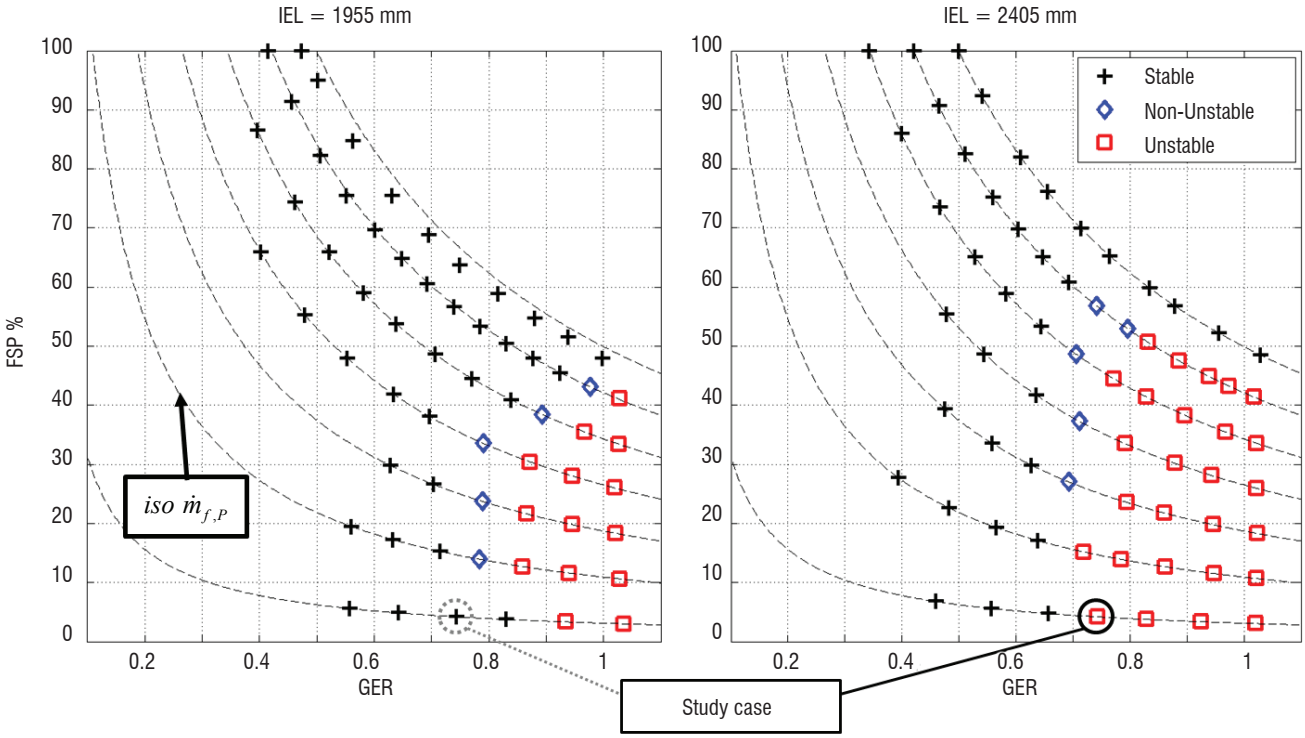

Figure 17 - LOTAR set-up stability map for IEL=1955 and 2405 mm, with $\dot{m}_{air}$ = 100 g/s, T_{air} = 473 K. [24]

Stability analysis

The influence of the Inner Exhaust Length (IEL) on the flame stability is illustrated in videos showing that, for a same flow condition, the flame changes from a stable condition for low IEL to unstable conditions for high IEL. A stability map of the setup with respect to the Global Equivalence Ratio (GER) and the fuel split ratio between the pilot and the multipoint zone was defined for two acoustic conditions corresponding to two IEL. The method used to define the stability criterion was inspired from the approach used by Samaniego et al. [35], which used the analysis of the pressure and flame radiation oscillations to identify the stability regime. From each signal, a stability map was drawn taking into account a threshold level for the fluctuation amplitude, delimiting the stable/unstable regions. As they conclude that a reasonably good overlapping of the unstable zones was deduced from each signal analysis, the definition of the combustion stability used on the LOTAR setup is based only on pressure fluctuation measurements. From a preliminary study, two criteria were used to define the flame stability: the sound pressure level of the resonant peak and the presence of at least one harmonic of the resonant frequency. The amplitude threshold was fixed at 145 dBSPL. Hence, three flame categories were defined. When both criteria are fulfilled, the flame is classified as "Unstable"; when no criterion is met, the flame is classified as "Stable"; and, finally, if only the amplitude criterion is met the flame is identified as "Non-Unstable".

The maps obtained for both IEL values are presented in Figure 17. The dash lines correspond to constant fuel mass flow rates through the pilot injector. It is noticeable that the uppermost line is always stable, which means that instabilities no longer appear if the fuel mass flow rate of the pilot injector is large enough. The unstable cases correspond to the region of higher global equivalence ratios, which is larger for IEL=2405 mm. As a result, as shown in the video, for some flow conditions, the flame changes from the stable to the unstable regime by modifying the IEL value.

The acoustic power $\vec{I}$ delivered by the setup can be used to quantify the coupling rate between the acoustics and the flame [36]. This acoustic power is defined by:

$$\vec{I} = \left\langle \left(1 + \frac{u_0^2}{c_0^2}\right) p\vec{u} + \vec{u}_0 \left(\rho_0 u^2 + \frac{p^2}{\rho_0 c_0^2}\right) \right\rangle$$

where $<>$ correspond to the temporal integration.

Munro and Ingard [37] developed a two-microphone technique enabling the acoustic power to be measured in ducts with a grazing air flow. This technique was applied on the LOTAR setup, by using the pressure signals measured on the two downstream taps located on the movable tube using a plane wave hypothesis. The influence of the IEL on the acoustic power delivered by the flame is plotted in Figure 18 for a fixed air and kerosene condition. It can be seen that the acoustic power increases greatly when the IEL increases. It reaches a maximum value for IEL around 2030 mm and then decreases.

The influence of the IEL on the growth rate was studied by Ghani [38] from a CFD approach, using the Helmholtz code AVSP (Figure 18). They observed a great increase in this parameter with the IEL The transition between the stable and the unstable configurations is obtained for IEL equal to 2350 mm. This comparison between the acoustic power and growth rate evolutions with respect to the IEL shows that the modification of this parameter changes the relationship between the pressure and the unsteady heat release in the chamber, leading to a great amplification of the acoustic energy delivered by the flame. It is noticeable that, for tube lengths below 2300 mm, even if the flame is still stable (growth rate negative), the acoustic power increases in

parallel to the growth rate. Furthermore, the higher acoustic power is reached close to the transition between the stable and unstable regimes

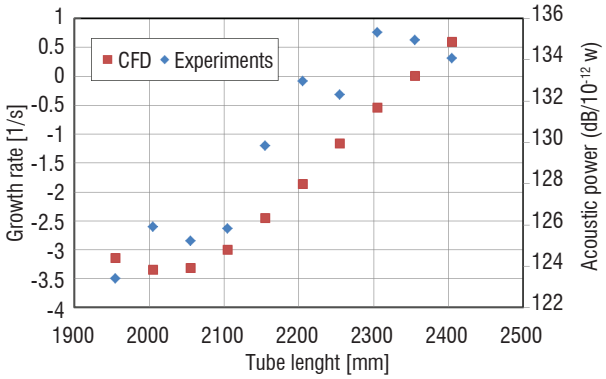

Figure 18 - Influence of the IEL on the acoustic power delivered by the combustion (Experiments) and the growth rate deduced from the CFD approach [38].

In order to complete this analysis on the interaction between the acoustic and the heat release from the flame, the local Rayleigh distribution, calculated from Eq. (2), is applied to the OH fluorescence results, similarly to the work of Samaniego et al. [34] and Lee et al. [39].

$$Ra(x,r) \propto \frac{1}{T}\int_{T} p'(x,r,t)q'(x,r,t)dt \qquad (2)$$

The computation of the local values is performed pixel by pixel, and yields the Rayleigh distribution displayed in Figure 19. For this representation, negative index values are represented in black, while positive ones are represented in red, and neutral ones are represented in white. Positive local Rayleigh index values mean that the local fluctuation of the unsteady heat release is in phase with the pressure fluctuation and therefore contributes to the combustion instability. On the other hand, the negative local Rayleigh index values indicate a stabilizing region, contributing to damp the instabilities due to unsteady heat release out of phase with the chamber pressure. A first conclusion that can be drawn from Figure 19 is that the IRZ (Inner Recirculation Zone), located in the flow region between the combustor longitudinal axis and the flame front (red area), sustains instabilities. Additionally, it reveals the position of the flame during the cycle. The flame angle is smaller during the first half of the pressure cycle, while this angle is wider during the second half of the pressure cycle, when the unsteady heat release is damping the instability phenomena (black area). Furthermore, the non-homogeneity of the Rayleigh index in the combustion chamber confirms the non-compact characteristic of the flame, as evidenced by LES simulations.

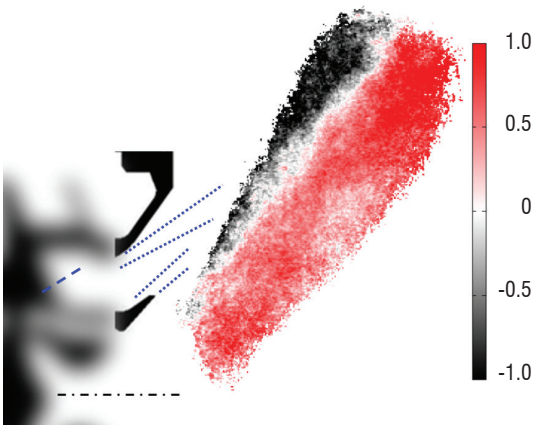

Figure 19 - Spatial distribution of the local Rayleigh index [24]

Conclusions and perspectives

Thermo-acoustic coupling is complex because many phenomena, such as combustion, chemistry, acoustic thermal transfer or one-phase or two-phase flow dynamics are involved. In many applications, this coupling may cause great pressure and heat release oscillations, which induce a risk for the safety of the systems involved. Many studies have been carried out over the years to understand and model the coupling lines and to develop numerical tools for predicting the appearance of instabilities and at last to try to prevent them. The key point of these models is certainly the measurement and, in parallel, the calculation of the time scales involved between the acoustic perturbations and the flame response. This analysis also shows that nonlinear phenomena in the flame response must be taken into account for an accurate description and, at last, prevention of the thermo-acoustic instabilities. Up to now, the flame response to acoustic excitations was determined from dedicated experiments performed on simplified configurations, mainly at low pressure. Their application to realistic conditions is not straightforward, because the pressure and the temperature may modify, even slightly, the flame position and structure which, finally, may have a drastic influence on the p'q' phase dependence. In order to improve this response identification, recent methods based on LES simulations have been proposed. Nevertheless, these simulations must accurately consider all of the individual phenomena involved in the $p'q'$ coupling, in order to obtain the right phase and amplitude response of the flame.

This paper is focused on applications dedicated to liquid-fueled aero engines. A description of the main approach found in the literature is proposed, with recent results obtained at ONERA where the liquid phase role in the $p'q'$ coupling is evidenced. It is shown that, depending on the injection method, various phenomena appearing between the fuel injection and its combustion can be taken into account in the models. The first concerned the response of the liquid phase to pressure or velocity oscillations close to the injection location. In this case, various flow patterns, such as liquid jet or liquid/wall interactions, must be considered. Other studies highlight that the heat release oscillations may be the result of the spray response to acoustic excitation. From these various works, it is evident that an accurate prediction of the combustion instability risks must take into account all of these phenomena. In particular, for liquid-fueled applications, the prediction of the flame response from the LES simulation can only be achieved if the unsteady behavior of the liquid phase is well modeled.

In order to achieve this objective, the ONERA project "Simulation des Instabilités de combustion Générées dans les Moteurs Aéronautiques et spatiaux (SIGMA)" was launched in 2015. In this project, the recent development of the multifluid approach in the ONERA CEDRE code (Refloch, 2011) will be used to calculate the response of the two-phase flow flames in aero engine and aerospace applications. In parallel, further experiments on the LOTAR setup will be performed to validate the simulations and to study in more details the non-linear response of the flame. The prediction of the combustion instability modes will be performed from both a low order approach and the Helmholtz code AVSP ■

References

[1] B. HIGGINS - *On the Sound Produced by a Current of Hydrogen Gas Passing Through a Tube*. Journal of Natural Philosophy, Chemistry and the Arts, 1, 129-131.

[2] P. RIJKE - *Notice of a New Method of Causing a Vibration of the Air Contained in a Tube Open at Both Ends*. Philosophical Magazine: Series 4, 17(116), 419-422.

[3] J. RAYLEIGH - *The Theory of Sound*. New York: Dover.

[4] D.J. HARRJE, F.H. READON - *Liquid Propellant Rocket Instability*. NASA SP 194.

[5] A.PUTNAM, W. DENNIS - *A Survey of Organ-Pipe Oscillations in Combustion Systems*. J. of Acoust. Soc. of America, 28(2), 246-259.

[6] F. NICOUD, T. POINSOT - *Thermoacoustic Instabilities: Should the Rayleigh Criterion be Extended to Include Entropy Changes?* Combustion and Flame, 142(1-2), 153-159.

[7] A. MINOTTI, F. SIMON, F. GANTIÉ - *Characterization of an Acoustic Liner by Means of Laser Doppler Velocimetry in a Subsonic Flow*. Aerospace Science and Technology, 12 , 398–407, doi:10.1016/j.ast.2007.09.007

[8] W. STRAHLE - *On Combustion Generated noise*. Journal of Fluid Mechanics, 49(2), 399-414.

[9] S. DUCRUIX, T. SCHULLER, D. DUROX, S. CANDEL - *Combustion Dynamics and Instabilities: Elementary Coupling and Driving Mechanisms.* Journal of Propulsion and Power, 19(5), 722-734.

[10] T. LIEUWEN - *Modeling Premixed Combustion-Acoustic Wave Interactions: A Review*. Journal of Propulsion and Power, 19(5), 765-781.

[11] F.E. MARBLE, S. CANDEL - *Acoustic Disturbance from Gas Non-Uniformity Convected through a Nozzle.* Journal of Sound and Vibration, 55(2), 225-243.

[12] W.POLIFKE, C.O. PASCHEREIT, K. DÖBBELING K - *Constructive and Destructive Interference of Acoustic and Entropy Waves in a Premixed Combustor with a Choked Exit.* International Journal of Acoustic and Vibration, 6(3), 135-146.

[13] M. HUET, A. GIAUQUE - *A non Linear Model for Indirect Combustion Noise Through a Compact Nozzle*. Journal of Fluid Mechanics, 733, 268-301.

[14] T. SATTELMAYER - *Influence of the Combustor Aerodynamics on Combustion Instabilities from Equivalence Ratio Fluctuations.* Journal of Engineering for Gas Turbines and Power 2003 125 (1), 2003, 11-19

[15] F. NICOUD, L. BENOIT, C. SENSIAU, T. POINSOT - *Acoustic Modes in Combustors with Complex Impedances and Multidimensional Active Flames*. AIAA Journal, 45, 426-441.

[16] A.P. DOWLING - *Nonlinear Self-Excited Oscillations of a Ducted Flame*. Journal of Fluid Mechanics, 346, 271-290.

[17] N. NOIRAY, D. DUROX, T. SCHULLER, S. CANDEL - *A Unified Framework for Nonlinear Combustion Instability Analysis Based on the Flame Describing Function*. Journal of Fluid Mechanics, 615, 139-167.

[18] E. GUTMARK - *Shear-Flow Role in Combustion Control*. A. I. Astronautics (Éd.), AIAA 97-2113. AIAA Fluid Dynamics Conference.

[19] S. HERMETH - *LES Evaluation of the Effects of Equivalence Ratio Fluctuations on the Dynamic Flame Response in a Real Gas Turbine Combustor Chamber.* Proceeding of the Combustion Institute, 3165-3173.

[20] T. LIEUWEN, B.T. ZINN - *Theoretical Investigation of Combustion Instability Mechanisms in Lean Premixed Gas Turbines*. AIAA-98-0641. American Society of Aeronautics and Astronautics.

[21] J. ECKSTEIN, E. FREITAG, C. HIRSCH, T. SATTELMAYER - *Experimental Study on the Role of Entropy waves in Low-Frequency Oscillations in a RQL Combustor.* Journal of Engineering for Gas Turbines and Power 128 (2), 2006, 264-270

[22] F. GIULIANI, P. GAJAN, O. DIERS, M. LEDOUX - *Influence of Pulsed Entries on a Spray Generated by an Airblast Injection Device : An Experimental Analysis on Combustion Instability Processes in Aeroengines.* Proceeding of the Combustion Institute, 29(1), 91-98.

[23] P. GAJAN, A. STRZELECKI, B. PLATET, R. LECOURT, F. GIULIANI - *Investigation of Spray Behavior Downstream of an Aeroengine Injector with Acoustic Excitation.* Journal of Propulsion and Power, 23(2), 390-397.

[24] J.M. APELOIG, H.X. D'HERBIGNY, F. SIMON, P. GAJAN, M. ORAIN, S. ROUX - *Liquid-Fuel Behavior in an Aeronautical Injector Submitted to Thermoacoustic Instabilities*. Journal of Propulsion and Power, 31(1), 309-319.

[25] F. GIULIANI - *Analysis on the Behaviour of an Aeroengine Air-Blast Injection*. Toulouse: PhD Thesis, ISAE.

[26] T.J. ANDERSON, W. PROSCIA, J.M. COHEN - *Modulation of a Liquid-Fuel Jet in an Unsteady Cross-Flow.* ASME Turbo expo 2001. New Orleans, Louisiana: ASME. Paper N° 2001-GT-0048.

[27] J. SONG, J.G. LEE - *Characterization of Spray Formed by Liquid Jet Injected Into Oscillating Air Crossflow*. ASME Turbo Expo. Montréal, Canada: ASME. Paper N° GT2015-43726.

[28] L. CROCCO, S. CHENG - *Theory of Combustion Instability in Liquid Properlant Motors.* (AGARDodograph, Éd.) London: Butterworths.

[29] S. ILLINGWORTH, M. JUNIPER - *When Will a Flame Describing Function Approach to Thermoacoustics Work Well?* International Conference on Sound and Vibration. Vilnius Lithuania.

[30] T. POINSOT, D. VEYNANTE - *Theoretical and Numerical Combustion*. 2nd Edition.Philadelphia, USA: R.T. Edwards.

[31] G.J. BLOXIDIDGE, A.P. DOWLING, P.J. LANGHORNE - *Reheat Buzz: an Acoustically Coupled Instability.* Part 2. Theory. Journal of Fluid Mechanics, 193, 445-473.

[32] P.J. LANGHORNE - *Reheat Buzz: an Acoustically Coupled Combustion Instability.* Part 1. Experiment. Journal of Fluid Mechanics, 193, 417-443.

[33] T. SATTELMAYER, W. POLIFKE - *Assessment of Methods for the Computation of the Linear Stability of Combustors.* Combustion Science and Technology, 175, 453-476.

[34] A. GHANI, L. GICQUEL, T. POINSOT - *Acoustic Analysis of a Liquid Fuel Swirl Combustor Using Dynamic Mode Decomposition*. ASME TURBO Expo 2015. Montréal: ASME. Paper N° GT2015-42769.

[35] J.M. SAMANIEGO, B. YIP, T. POINSOT, S. CANDEL - *Low-Frequency Combustion Instability Mechanisms in a Side-Dump Combustor.* Combustion and Flame, 94, 363-380.

[36] C.L. MORFEY - *Acoustic Energy in Non Uniform Flows*. Journal of Sound and Vibration, 14, 159-170.

[37] D.H. Munro, K.U. Ingard - *On Acoustic Intensity Measurements in the Presence of Mean Flow*. J. Acoust. Soc. Am., 65 (6), 1402-1406.

[38] A. GHANI - *LES of Self Excited Transverse Combustion Instabilities in Perfectly-Premixed and Swirling Spray Flames*. Ph D, Université de Toulouse. 'http://oatao.univ-toulouse.fr/15658/1/ghani.pdf '

[39] S.-Y.LEE, S. SEO, J.C. BRODA, S. PAL, R.J. SANTORO - *An Experimental Estimation of Mean Reaction Rate and Flame Structure During Combustion Instability in a Lean Premixed Gas Turbine Combustor.* Proceedings of the Combustion Institute, 28(2), 775-782.

[40] A.C. REFLOCH - *CEDRE Software.* (ONERA, Ed.) Aerospace Lab Journal(2), 1-10.

Nomenclature

Σ	=	surface of the control system boundary, m^2
Ω	=	volume of the control system, m^3
γ	=	heat capacity ratio
ρ	=	density, kg/m^3
τ	=	characteristic time, s
ω	=	pulsation angle, rad/s
ϕ	=	equivalence ratio
c	=	sound velocity, m/s
dA	=	surface integration variable, m^2
dt	=	time integration variable, s
dV	=	volume integration variable, m^3
D_{REF}	=	reference diameter
FDF	=	Flame Describing Function
FSP	=	Fuel Split Parameter
FTF	=	Flame Transfer Function
GER	=	Global Equivalence Ratio
I	=	light intensity over camera dynamics, # counts
IEL	=	Inner Exhaust Length, mm
J	=	momentum ratio
L	=	distance, m
$\dot{m}_{air}$	=	air mass flow rate, g/s
$\dot{m}_{f,P}$	=	fuel mass flow rate on the pilot system, g/s
$\dot{m}_{f,MP}$	=	fuel mass flow rate on the multipoint system, g/s
n	=	interaction index
p'	=	acoustic pressure, Pa
$\overline{P}$	=	averaged pressure, Pa
q'	=	unsteady heat release, W/m^3
Q	=	total heat release produced by the flame, W
Ra	=	local Rayleigh index
S	=	Surface, m^2
T	=	instability cycle period, s
T_{air}	=	air inlet temperature, K
u'	=	acoustic velocity, m/s

AUTHOR

Frank Simon graduated from ENSICA Toulouse with a degree in Aeronautical Engineering (1989), from Supaero Toulouse with a PhD in Mechanical Engineering (Acoustics) (1997) and from the University of Toulouse with Authorization to supervise PhD students (2007). He is a Research Master at Onera, specialized in the development of vibro-acoustic modeling and measurement techniques and has participated in various EC projects in the vibro-acoustic domains (RHINO, FACE, FRIENDCOPTER), as well as being in charge of internal noise in the Garteur group.

Mikael ORAIN received his Masters degree in fluid mechanics in 1996 and his PhD in Mechanical Engineering in 2001 from the Imperial College London (UK). He is a research scientist at ONERA/DMPH in charge of developing PLIF for the measurement of temperature and species concentrations in reacting and non-reacting two-phase flows.

Pierre GAJAN received the degree of Doctor of the University of Rouen in 1983 and that of Science Doctor in 1988. He has worked as a research engineer at ONERA since 1987 as an experimentalist and is in charge of the research unit on multiphase flows in the department of "Models for Aerodynamics and Energetics" since 2008. He has carried out many projects on flow dynamics in pipes, first under mono-phase conditions and then in two-phase flows for the gas industry. Since 2000, he has worked on combustion instabilities in order to analyze the role of the liquid phase on the thermoacoustic couplings.

Virginel BODOC graduated from the Military Technical Academy of Bucharest in 2003. In the following years, he worked as a Research Engineer at the Military Equipment and Technology Research Agency of Bucharest. After obtaining a Master Degree Diploma from the INP Toulouse in 2007, he joined ONERA as a Marie Curie doctoral fellow and defended his PhD in 2011. Since 2010, he has been involved in various research projects conducted at the LACOM combustion laboratory (Fauga-Mauzac center). Within the research team, his main field of activity is the development and application of optical measurement techniques (PIV, PDA/LDA, LIF, Rainbow Refractometry and Infrared Absorption) to characterize reacting and non-reacting gas/droplet flows. Since 2013 he has been in charge of the LACOM facility technical survey.